



## **A new technique for real-time measurements of potassium and sodium aerosols based on field-reversal surface ionization**

Downloaded from: <https://research.chalmers.se>, 2025-12-04 16:04 UTC

Citation for the original published paper (version of record):

Gall, D., Nejman, C., Allgurén, T. et al (2021). A new technique for real-time measurements of potassium and sodium aerosols based on field-reversal surface ionization. *Measurement Science and Technology*, 32(7).  
<http://dx.doi.org/10.1088/1361-6501/abe130>

N.B. When citing this work, cite the original published paper.

PAPER • OPEN ACCESS

# A new technique for real-time measurements of potassium and sodium aerosols based on field-reversal surface ionization

To cite this article: Dan Gall *et al* 2021 *Meas. Sci. Technol.* **32** 075802

View the [article online](#) for updates and enhancements.

## You may also like

- [Study on the Harm of Saline Alkali Land and Its Improvement Technology in China](#)  
Baoqiang Zhang and Na Wang
- [Solution- Processed Alkali Metals-Doped Amorphous Zinc Tin Oxide Thin-Film Transistors and Analysis of Alkali Metal Doping Mechanism through the UV-Visible Spectroscopic](#)  
Keon-Hee Lim, Eungkyu Lee, Kyongjun Kim *et al.*
- [Lifecycle assessment of alkali activated cement concrete](#)  
Angitha K Viswanath and K B Anand



The Electrochemical Society  
Advancing solid state & electrochemical science & technology

242nd ECS Meeting

Oct 9 – 13, 2022 • Atlanta, GA, US

Abstract submission deadline: **April 8, 2022**

Connect. Engage. Champion. Empower. Accelerate.


**MOVE SCIENCE FORWARD**



Submit your abstract



# A new technique for real-time measurements of potassium and sodium aerosols based on field-reversal surface ionization

Dan Gall<sup>1,3</sup> , Charlotta Nejman<sup>1</sup>, Thomas Allguren<sup>2</sup>, Klas Andersson<sup>2</sup> and Jan B C Pettersson<sup>1</sup>

<sup>1</sup> Department of Chemistry and Molecular Biology, University of Gothenburg, Gothenburg, Sweden

<sup>2</sup> Department of Space Earth and Environment, Chalmers University of Technology, Gothenburg, Sweden

E-mail: [dan.gall@chalmers.se](mailto:dan.gall@chalmers.se)

Received 15 November 2020, revised 18 January 2021

Accepted for publication 28 January 2021

Published 30 April 2021



## Abstract

A new method for real-time measurements of potassium and sodium containing aerosol particles is described and verified. The method is based on surface ionization technique and may be used to explore the alkali chemistry related to high temperature chemistry processes. The measurement device is a further development of the simple and cost-effective surface ionization detector previously used for online alkali measurements in combustion and gasification research. The discrimination between sodium and potassium is possible due to differences in their surface desorption kinetics and facilitated by rapidly reversing the field potential between the ion source and the nearby collector. The instrument is evaluated in a series of laboratory experiments using size-selected alkali salt particles containing KCl, NaCl, K<sub>2</sub>SO<sub>4</sub>, Na<sub>2</sub>SO<sub>4</sub>, KNO<sub>3</sub> and NaNO<sub>3</sub>. The filament temperature was found to be a key influencing factor in order to optimize the strength and Na–K deviation of the observed ion current. The ability to simultaneously report absolute concentrations of Na and K makes the instrument attractive for solid fuel conversion of alkali-rich fuels such as low-grade biomass and to explore behavior deviations of Na and K in high temperature processes.

Keywords: alkali, aerosols, ionization, combustion, corrosion

(Some figures may appear in colour only in the online journal)

## 1. Introduction

The use of biogenic fuels in combined heat and power generation is an efficient CO<sub>2</sub> mitigation option and the

interest in alternative energy sources, such as biomass and waste-based fuels, has increased drastically in recent years [1]. The two main subcategories of biomass that are commonly used as fuel for heat and power generation purposes are forest-derived and agriculture-derived biomass. The composition of different types of biomass will differ considerably regarding moisture, reactivity and ash composition. However, in general, there are even larger differences in the composition of biomass compared to other solid fuels such as coal. In particular, the high alkali content, sodium and potassium, is considered problematic when using biomass fuels. Alkali matter is transformed in the combustion process and forms corrosive

<sup>3</sup> Author to whom any correspondence should be addressed.



Original content from this work may be used under the terms of the [Creative Commons Attribution 4.0 licence](https://creativecommons.org/licenses/by/4.0/). Any further distribution of this work must maintain attribution to the author(s) and the title of the work, journal citation and DOI.

salts, salts that may deposit on heat transfer surfaces and cause high-temperature corrosion (HTC).

Compounds that contain alkali metals and chlorine are among the most aggressive agents, which is why HTC is primarily a problem for power plants that are fired with biomass rather than coal [2–4]. To counteract HTC in biomass-fired power plants, the steam temperature in the boiler is often lowered, which leads to a decreased electrical efficiency [5]. The risk for alkali-related HTC can be reduced by the co-combustion of coal and biomass (relative to the combustion of biomass alone) owing to the relatively high levels of fuel-bound sulfur in coal, which favors the formation of the less-corrosive sulfates over chlorides [6–8].

The key inorganic elements related to HTC are sulfur, chlorine, potassium and sodium, which is released during combustion and devolatilization. Their relative rates of release and in which form they are released are, however, highly dependent upon the overall fuel composition and temperature. Sodium and potassium will mainly be released as chlorides (NaCl/KCl) in the presence of Cl, in their atomic form (Na/K) or as hydroxides (NaOH/KOH) [9–12]. In general, the transformation and specific reactions of Na and K species are assumed similar in combustion atmospheres. In the work of Glarborg and Marshall [13] the platform for the existing gas-phase alkali sulfation mechanism is established and it is worth noting that only a few reactions between Na and K species with Cl and S compounds were based on direct measurements. In fact, due to the lack of experimental data, the recombination reactions between Na/K and SO<sub>2</sub> are the only sulfation reactions that are based on direct measurements in the mechanism. Thus, there is a need for new experimental approaches that can provide Na and K release rates in the combustion process in order to establish improved knowledge on the sulfation and chlorination sequences critical to HTC.

Several alkali measurement techniques have been applied in combustion chemistry research [14–19]. *In-situ* optical measurements provide comprehensive molecular data with satisfactory time and space resolution to study the detailed combustion chemistry. Reported techniques include, but are not limited to; absorption spectroscopy, light scattering, and fluorescence. A recent summary can be found in [20]. While some optical diagnostic tools required conditional information to deliver absolute concentration, others, such as tuneable laser absorption spectroscopy rely on the reduced transmitted intensity. However, application of optical techniques in industrial settings may be hindered by the optical density in the sample flow and the harsh external environment (i.e. temperature fluctuations, vibrations and contaminations) associated with high temperature process plants. Consequently, extractive methods that relies on particle collection and subsequent chemical analysis are still widely used. Other applied techniques rely on continuous extraction, where the sample gas is conditioned, diluted and continuously fed to the analyzer, typically a mass spectrometer with various ionization methods. So called soft ionization techniques dissolve the aerosols, enabling detection of individual chemical constituents, however, this type of ion-formation may increase uncertainties coupled to stability of the ion signal [21, 22]. Other

high intensity ionization processes, such as plasma technique, provide a stable ion signal while losing the detailed molecular information [23]. However, limited portability, large investment cost and the need of a qualified operator compose limitations for implementing such measurement techniques.

A simple and low-cost alternative is the surface ionization detector (SID) based on surface ionization (SI) to measure the total alkali concentration (K + Na). The method lends itself to be used in particle-laden systems such as biomass combustion and have previously been applied in combustion and gasification research [24–28]. However, without the ability to distinguish between Na and K, thus reporting only the combined alkali concentration.

We herein describe a new field reversal SID (FR-SID) that may be used to determine the mass concentration per volume of potassium and sodium separately. Rapid reversal of the electric field outside the hot Pt filament in the SID allows us to distinguish between Na and K based on differences in their desorption kinetics. The work builds on previous studies using the field reversal technique for alkali atom desorption from metal surfaces [29–31], with the aim to develop a low-cost alkali detector able to report absolute mass concentrations (g m<sup>-3</sup>). The estimated cost for this type of instrument is ~15 k USD (based on year 2020 buying power). Results from laboratory studies with size-selected alkali salt particles are presented, including KCl, NaCl, K<sub>2</sub>SO<sub>4</sub>, Na<sub>2</sub>SO<sub>4</sub>, KNO<sub>3</sub> and NaNO<sub>3</sub>.

## 2. Methods

### 2.1. SI

SI is a naturally occurring phenomenon in which adsorbed atoms or molecules are ionized during thermal desorption [32]. The ratio between the desorbing fluxes in ionic and neutral form can be predicted by the Saha–Langmuir equation [32, 33] where the degree of ionization ( $\alpha$ ) is

$$\alpha = \frac{n_+}{n_0} = \frac{g_+(1-r_+)}{g_0(1-r_0)} \exp \left[ \frac{e(\phi - \text{IP})}{k_B T} \right], \quad (1)$$

where  $n_+$  is the number of positive ions leaving the surface area per second and  $n_0$  is the number of neutral atoms emitted from the same surface element in the same time.  $g_0/g_+$  denotes the statistical sum ratio of neutral atoms and ions ( $g_0/g_+ = 2$  for alkali metals) and  $e\text{IP}$ ,  $e\phi$ ,  $k_B$  and  $T$  are the ionization potential of the desorbing species (eV), surface work function (eV), Boltzmann's constant (eV K<sup>-1</sup>) and surface temperature (K), respectively. The reflection coefficients  $r_0$  and  $r_+$  are in general close to zero. The ionization probability ( $\beta$ ) of a species is obtained by

$$\beta = \alpha / (\alpha + 1). \quad (2)$$

For most atoms and molecules  $\text{IP} > \phi$  and the emission of neutral species from the surface is strongly favored over ion desorption. However, ion emission is favored when  $\text{IP} < \phi$ , which is often the case for alkali metals. Figure 1 shows ionization probabilities for a few selected elements on a 1500 K

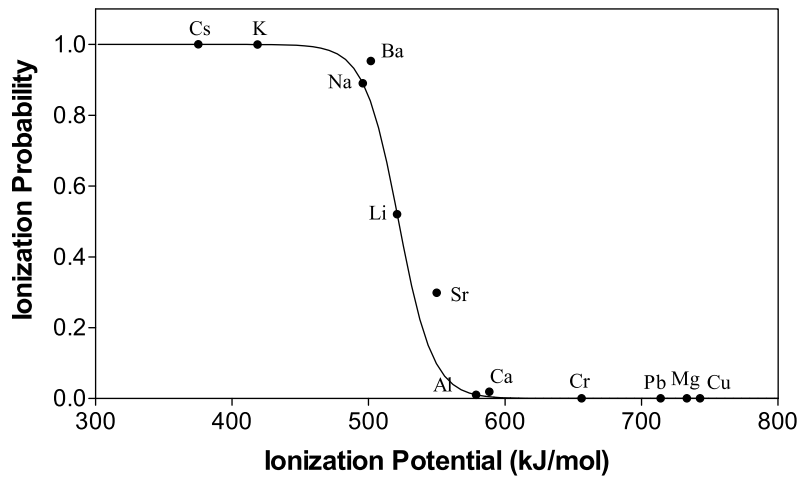


**Figure 1.** Surface ionization probability versus ionization potential for selected elements according to equation (2). The ionizing surface was assumed to have a work function  $\phi = 530 \text{ kJ mol}^{-1}$  (corresponding to polycrystalline platinum) and a surface temperature  $T = 1500 \text{ K}$ . The solid line represents elements with the statistical sum ratio of neutral atoms and ions  $g_0/g_+ = 2$ .

platinum surface with  $\phi = 530 \text{ kJ mol}^{-1}$  [34]. The valence electron of the alkali atoms preferably remain on the metal surface during the thermal desorption process, and the ionization probabilities of Na (89%) and K (>99%) are high. Other alkali metals are also easily ionized, however, concentrations are usually low compared to the abundant sodium and potassium. Alkaline earth elements may also desorb in ionic form, although their binding energy to platinum is substantially higher than for the alkali metals and their desorption rate is negligible at temperatures below 1500 K [35].

In an SID, the SI process is used to achieve selective detection of alkali metals. An SID consists of a metal filament on which alkali metals are ionized and a nearby metal plate that acts as an ion collector [29, 36]. These are situated in parallel a few millimeters apart and are enclosed in the measurement cell. The filament is resistively heated to high temperature and is kept at a positive potential of a few hundred volts while the nearby ion collector is grounded. As an alkali-containing aerosol flows through the cell some particles interact with the hot filament. This causes salt particles to dissociate and the formed atoms adsorb on the surface. A large fraction of the adsorbed alkali metal atoms subsequently desorb as ions, while anions either create bonds with the surface or form volatile compounds that evaporate. The alkali ions are carried by the electric field to the nearby ion collector and give rise to an electron pulse that is amplified and measured [37].

## 2.2. The field reversal method

Earlier work has shown that rapid electric field reversal (FR) outside an ionizing metal surface may be used to investigate the desorption kinetics of alkali ions on surfaces under atmospheric pressure [29, 37], which drastically reduce the complexity and costs compared to vacuum systems. The main idea of the FR method is to periodically block the ionic desorption channel by changing the direction of the electric field outside the surface. If a retarding field is applied, desorbed ions will be forced to the filament surface.

The basic principle of the FR technique is illustrated in figure 2, where a constant flux of alkali is assumed to reach the surface at all times, i.e. flue gas from alkali containing fuels. During the retarding phase when a negative potential is applied to the ionizing filament, the surface concentration of alkali atoms increases since the desorption is limited to neutral alkali atoms. As the electrical field is switched to the accelerating phase the surface concentration decreases due to desorption of both neutrals and ions, until a steady state is reached where the constant flux to the surface is balanced by the constant flux of emitted alkali ions and atoms.

The rate equations that describe the surface concentrations during the accelerating and retarding phases can be described by [38]

$$\frac{dc_s(t)}{dt} = f - (k_+ + k_0)c_s(t) \quad \text{accelerating phase} \quad (3)$$

$$\frac{dc_s(t)}{dt} = f - k_0c_s(t) \quad \text{retarding phase} \quad (4)$$

where  $c_s(t)$  is the surface concentration (number of adsorbed atoms per area),  $f$  is the incoming flux of alkali metal atoms ( $\text{s}^{-1}$ ), and  $k_+$  and  $k_0$  are the ionic and neutral rate constants for desorption ( $\text{s}^{-1}$ ), respectively. The solutions of the differential equations are

$$c_s(t) = \frac{f}{k_+ + k_0} - \left( \frac{f}{k_+ + k_0} - c'_s(0) \right) \times \exp[-(k_+ + k_0)t] \quad \text{accelerating phase} \quad (5)$$

$$c_s(t) = \frac{f}{k_0} - \left( \frac{f}{k_0} - c''_s(0) \right) \exp[-k_0t] \quad \text{retarding phase} \quad (6)$$

where  $c'_s(0)$  and  $c''_s(0)$  are the initial surface concentrations during the accelerating and retarding phase, respectively. The desorbing flux is at all times proportional to the surface



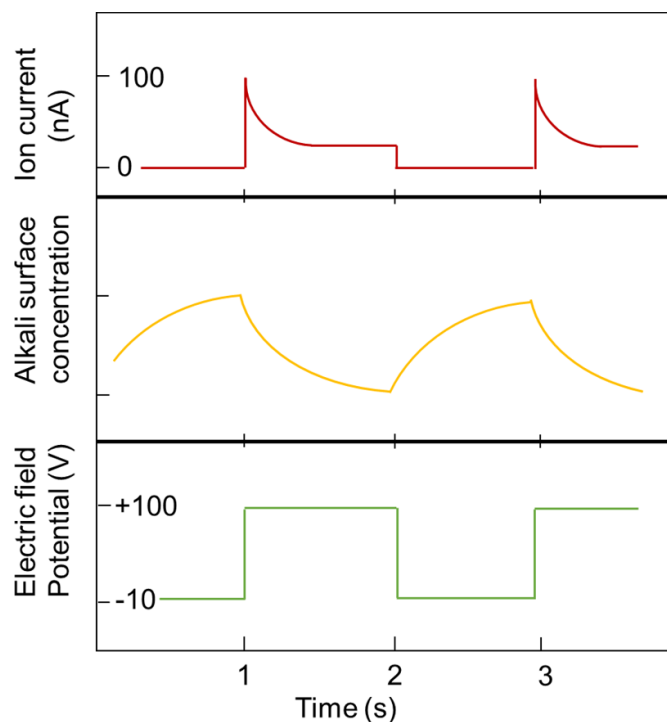


**Figure 2.** Basic principle of the FR technique. The figure shows an example of the time variation of the surface potential, the surface concentration of alkali atoms (in arbitrary units), and the measured SID current. A constant incident flow of alkali is assumed to reach the ionizing surface at all times.

concentration, and  $k_+$  and  $k_0$  can be determined from the time-dependence of the signal due to desorbing species.

The FR method has previously been used to study desorption kinetics from metal and metal oxide surfaces in vacuum and in air [29, 37, 38]. More recently, the desorption rate constants of  $\text{Na}^+$ ,  $\text{K}^+$  and  $\text{Cs}^+$  have been determined for metal surfaces in air [29, 37]. The general trend is that  $k_{\text{Na}^+} < k_{\text{K}^+} < k_{\text{Cs}^+}$ , meaning that  $\text{Na}^+$  desorbs slower than both  $\text{K}^+$  and  $\text{Cs}^+$  at a specific surface temperature. These differences in desorption kinetics open up the possibility to differentiate between  $\text{Na}^+$  and  $\text{K}^+$  based on differences in desorption rate, and this option is evaluated as an option for discrete measurements of Na and K concentrations in a sample gas.

### 2.3. Instruments, materials and experimental procedure

The FR-SID used in the present study is illustrated in figure 3, and a schematic view of the electrical control and data acquisition system is shown in figure 4. The SI detector consists of a resistively heated platinum filament (diameter 0.35 mm, purity 99.997%) and an stainless steel ion collector plate at a distance of 3 mm. Earlier studies have shown that polycrystalline platinum may remain stable under oxidized conditions [29], depending on surface temperature and oxygen pressure. The filament and the collector are housed in a cylindrical stainless steel cell with a length of 70 mm and a diameter of 70 mm. The cell is equipped with a quartz window in order to enable

optical temperature readings with a pyrometer, and the heating current is calibrated against the pyrometer in order to control the filament temperature. Joule heating is determined by the square of the current and can therefore be controlled with high precision, assuming that the reference point is accurate. Similar technique has been used in previous investigations and appears to be adequate. The detector plate is connected to a current amplifier (Model 427, Keithley Inc.) and the signal is registered by an oscilloscope and logged by computer. A function generator coupled to a switch circuit is used to alternate the field strength and direction at the filament surface, and the time period is set to 1 s for both the retarding and the accelerating phase, resulting in 0.5 Hz sampling frequency. A constant gas flow rate through the FR-SID, limited by a critical orifice, is maintained by an external pump during the experiments. The flow rate was verified before and after each experiment with a mass flow meter. The standard FR-SID operating parameters used in this study are listed in table 1.

For all evaluation experiments a constant output atomizer (Model 3076, TSI Inc.), operated in re-circulation mode, followed by a diffusion dryer was used to generate a stable flow of submicron alkali salt particles. Similar setup has been used in previous investigations of alkali salt particles with satisfactory purity and robustness [39]. The synthesized aerosols were produced from dissolved salts used as received from Merck & Co., Inc. with the following purity: KCl (>99.9%), NaCl (99.9%),  $\text{KNO}_3$  (99%),  $\text{NaNO}_3$  (99%),  $\text{K}_2\text{SO}_4$  (99.9%)  $\text{Na}_2\text{SO}_4$  (99.9%). For the aerosol verification a set of commercial aerosol instruments were used. A scanning mobility particle sizer (SMPS) was used to determine particle size distributions in the range 10–500 nm and to pre-select particles of a given size during laboratory evaluation of the FR-SID when a monodisperse aerosol was used. The SMPS consists of a differential mobility analyzer (DMA) (Model 3081, TSI Inc.) and a condensation particle counter (Model 3775, TSI Inc.). In addition, the size distribution and concentrations of particles were analyzed using an optical spectrometer (Model 1.108, GRIMM Aerosol Technik GmbH), which detects particles in the size range from 0.3 to 20  $\mu\text{m}$ .

## 3. Results and discussion

Figure 5 shows typical ion emission curves for  $\text{K}^+$  ions at eight different filament temperatures. Potassium was admitted to the FR-SID in the form of a monodisperse KCl aerosol, and all parameters (except temperature) were set to the standard conditions listed in table 1. The rapid change in filament voltage from  $-10$  to  $+300$  V at time zero induces a current peak in the ion collector plate. The induced transient current disturbs ion measurements on the time scale shorter than a few ms, but can largely be discriminated by adjusting the rise time of the amplifier and becomes insignificant at longer times. The amplifier is also initially saturated at the highest temperatures due to the combined effect of the induced current peak and ions reaching the collector. The ion emission affects the surface potassium population, which decreases to a new and lower steady state level according to equation (5). The decay

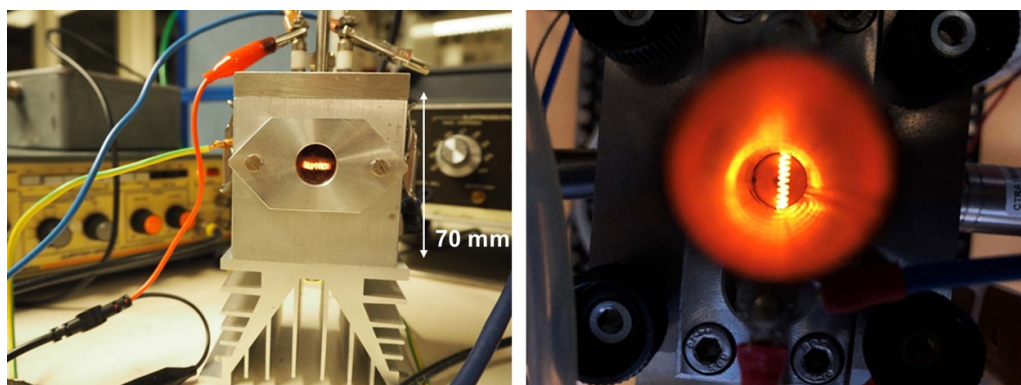


**Figure 3.** Left: Photo of the FR-SID measurement cell. Associated electronics can be seen in the background. Right: Close-up on the Pt-filament, heated to 1500 K, observed from the sample inlet. Aerosol particles will melt and ionize upon impact on the hot surface and collected by the detector plate (not visible).

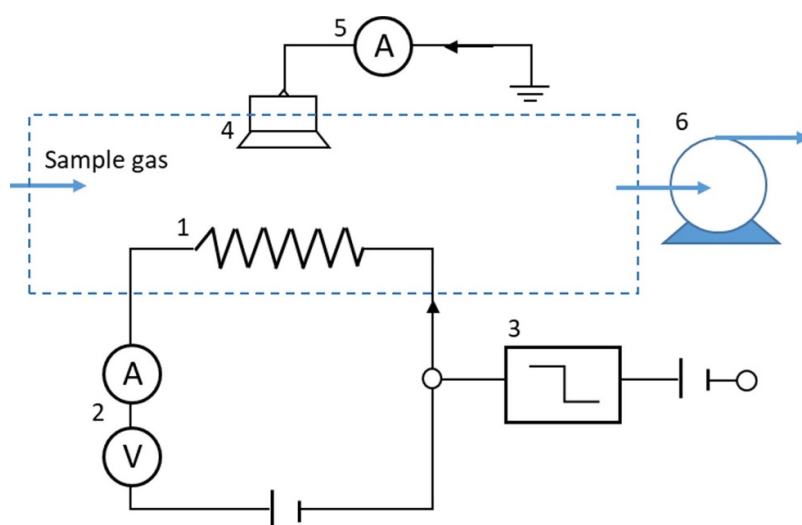


**Figure 4.** Schematic view of the FR-SID setup: 1. Pt filament; 2. filament current control; 3. wave generator; 4. collector plate; 5. ion current monitor; 6. pump.

in ion emission proceeds more rapidly when the filament temperature is raised from 1240 to 1490 K, which indicates that the rate constant for ion desorption increases with increasing temperature.

Figure 6 shows a comparison between the desorption kinetics of  $\text{Na}^+$  and  $\text{K}^+$  at a filament surface temperature of 1460 K. Both salts were individually admitted to the FR-SID as pure alkali chloride particles and the experimental conditions were otherwise identical. The potassium ion desorption is considerably faster than sodium ion desorption reflecting a lower stability of potassium on the surface. Least square fits of the decay curves using equation (5) result in desorption rate constants of 10 and  $97 \text{ s}^{-1}$  for  $\text{Na}^+$  and  $\text{K}^+$ , respectively, and the desorption rates thus differ by approximately a factor of ten at this temperature.

Measurements on KCl and NaCl particles were performed at filament temperatures between 1230 K and 1500 K with all other parameters set to standard conditions. The decay curves can in general be described by an exponential function and the data have been fitted by equation (5) to determine rate constants for desorption. The desorption rate constants

**Table 1.** Standard conditions and instrument parameters used during the FR-SID measurements.

Filament voltage during ion acceleration ( $U_{\text{acc}}$ )	+300 V
Filament voltage during ion retardation ( $U_{\text{ret}}$ )	−10 V
Length of accelerating and retarding phases	1 s
Filament temperature	1490 K
SID pump flow	$0.7 \text{ l min}^{-1}$
Salt solution and concentration	KCl, 1 mM
Diameter of monodisperse particles ( $d_p$ )	200 nm

are presented as an Arrhenius plot in figure 7. For KCl the rate constants ranged between 2 and  $117 \text{ s}^{-1}$  in the temperature range from 1230 to 1480 K, and for NaCl rate constants between 3 and  $22 \text{ s}^{-1}$  were determined in the range from 1400 to 1500 K.

In general, the temperature range where rate constants could be determined was smaller for Na salts than for K salts. At low temperatures the slow  $\text{Na}^+$  decay decreased the intensity, and noise made it impossible to fit an exponential equation to the decay on a time scale of 1 s. Below a

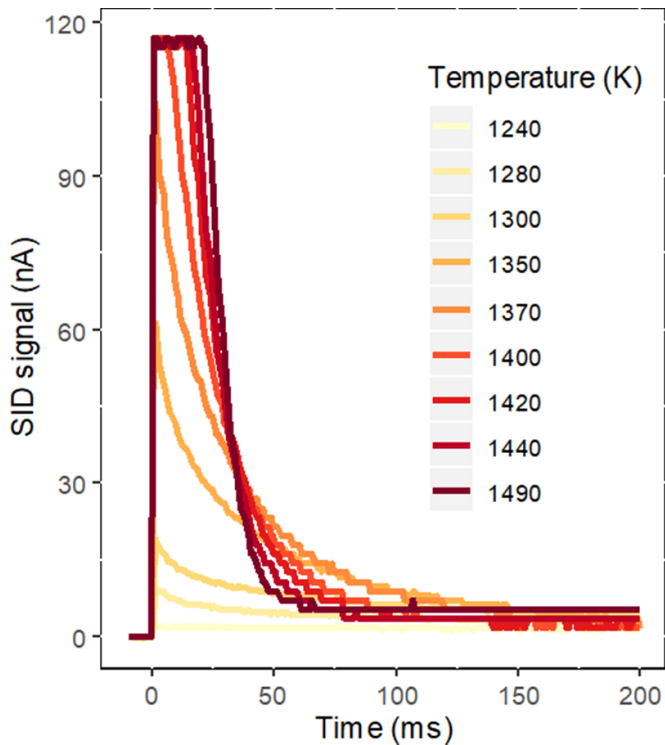


**Figure 5.** SID currents obtained from FR measurements on KCl particles at eight different filament temperatures during the first 200 ms of the 1000 ms accelerating phase.

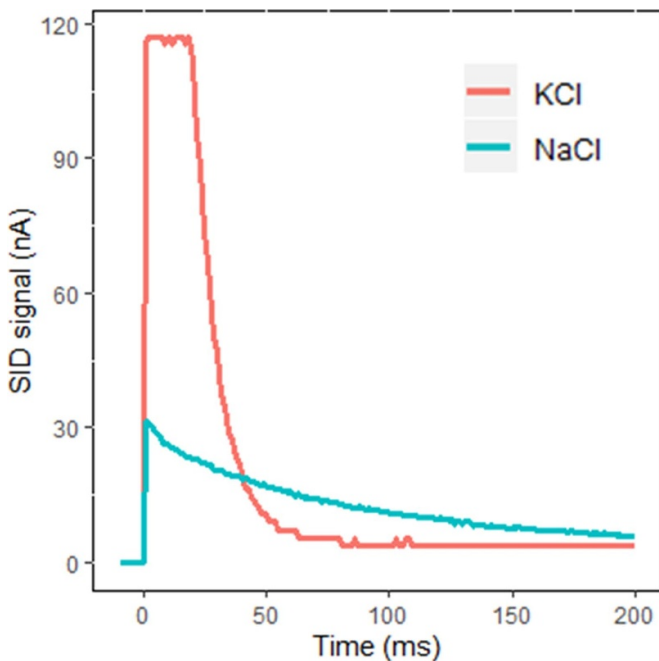


**Figure 6.** SID currents obtained from FR measurements on KCl and NaCl particles at filament temperature of 1460 K. The difference in desorption kinetics are used to discriminate between respective Na and K signals.

filament temperature of approximately 1400 K the observed rate constant for Na started to shift towards the K rate constant and are considered as not applicable. This indicates that a background level of K was present in the FR-SID, and at a

certain filament temperature the  $\text{Na}^+$  desorption rate became too slow and a background signal due to  $\text{K}^+$  desorption exceeded the  $\text{Na}^+$  signal. The background level of K may have originated from the filament itself, which contains minor inorganic inclusions from the metal production and emits some alkali metal ions during the first period of usage. The received NaCl used for the aerosol generation may contain up to 5 ppm of K, which constitutes another potential source of contamination. It is, however, also likely that some potassium remained in the FR-SID from prior laboratory experiments with potassium salts.

As seen in figure 7, the temperature dependence of the rate constants is linear in a wide range, which indicates that desorption of Na and K can be described by the Arrhenius equation:

$$k = Ae^{-E_a/(k_b T)}, \quad (7)$$

where  $A$  is a frequency factor and  $E_a$  is the activation energy (eV) for the desorption process. By fitting linear equations to the data in figure 7 the desorption energy (frequency factor) of  $\text{K}^+$  and  $\text{Na}^+$  were determined to 2.60 eV ( $8.8 \times 10^{10} \text{ s}^{-1}$ ) and 3.51 eV ( $1.2 \times 10^{13} \text{ s}^{-1}$ ), respectively.

In an earlier study Hagström *et al* [29] studied  $\text{K}^+$  desorption from platinum in air and reported desorption rate constants that were typically about three orders of magnitude higher than observed here. Arrhenius parameters agreed favorably with earlier studies of K–Pt interactions in vacuum [37], and the results were consistent with ordinary alkali ion desorption from the Pt crystal plane. We therefore performed additional experiments aiming at the identification of the fast desorption process characterized by Hagström *et al* [29], and concluded that it can be observed under experimental conditions that are similar to the ones used in the earlier study. In particular, the use of a high alkali mass concentration to the FR-SID is an important factor for the fast desorption to be visible with the simplified design used within this work. However, the interest in a low-cost alternative, with simplified deployed electronics, sought to improve our understanding of the setup used in the current study, where only the slow desorption is detectable.

Grain boundaries and irregularities are common on polycrystalline surfaces and may provide binding sites where alkali atoms are more strongly bound compared to sites available on a perfect crystalline surface. The slow desorption kinetics observed in the present study are consistent with the description that alkali atoms populate strongly bound states on the platinum surface, and the desorption from these sites is likely to go through an intermediate step where alkali atoms or bound to the crystal plane. The desorption kinetics for systems that involve multiple surface states are complex and known to produce Arrhenius parameters that deviate substantially from those found in ordinary desorption [40].

To assess the response for internally mixed aerosols, FR-SID measurements were carried out with internally mixed NaCl:KCl particles using a 50:50 molar mixture. The ion desorption curves were in general well described by a linear combination of two exponential functions describing the independent desorption of K and Na:



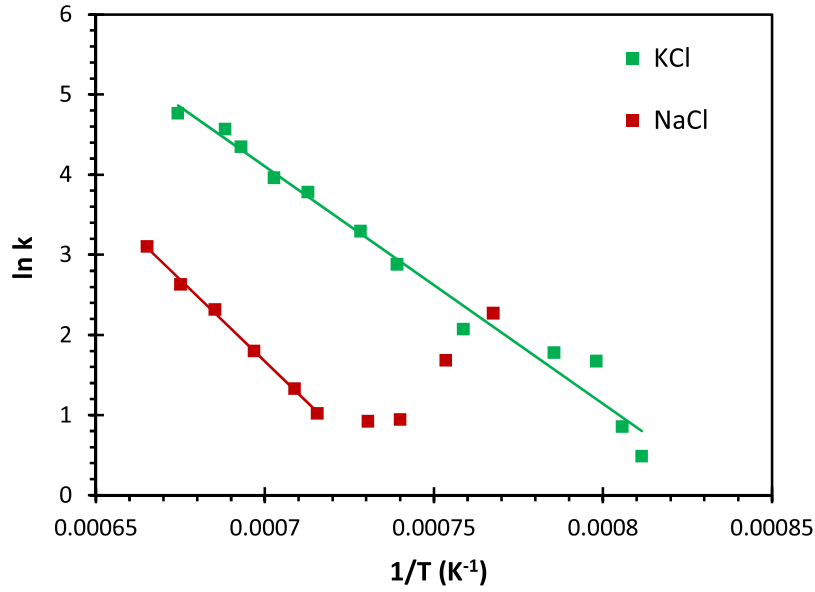


**Figure 7.** Arrhenius plot of desorption rate constants obtained in experiments with KCl and NaCl aerosol particles. Arrhenius parameters calculated from least-square fits of the data are listed in table 2. The linear region where the Arrhenius equation is valid are indicated with trend lines. At temperatures <1400 K the  $\text{Na}^+$  desorption becomes slow and the signal shift towards  $\text{K}^+$  desorption due to contamination.

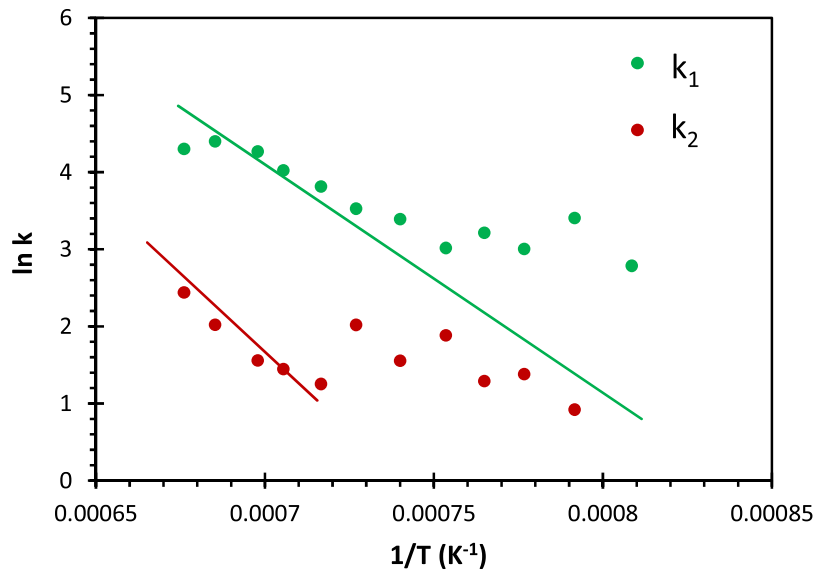


**Figure 8.** Arrhenius plot of desorption rate constants  $k_1$  and  $k_2$  obtained by fitting equation (8) to desorption data for internally mixed NaCl:KCl particles. The straight lines obtained from pure KCl and NaCl particles (see figure 7) are added as comparison.

$$I(t) = I_{01} e^{-k_1 t} + I_{02} e^{-k_2 t} + C, \quad (8)$$

where  $I_{01}$  (A) and  $I_{02}$  (A) are the initial currents measured by the FR-SID at time zero, where  $k_1$  ( $\text{s}^{-1}$ ) and  $k_2$  ( $\text{s}^{-1}$ ) are desorption rate constants and  $C$  (A) is an added constant to improve the fit. The obtained rate constants were found to resemble the results for pure NaCl and pure KCl (figure 7). As seen in figure 8,  $k_2$  describes the  $\text{Na}^+$  desorption down to a filament temperature of 1400 K and at lower temperatures the constants shift towards the K values. For pure NaCl particles the shift towards K values started at a similar temperature (figure 7). At lower temperatures  $k_1$  also starts to deviate from the pure KCl data. It is likely that  $k_1$  and  $k_2$  at low temperatures

describe different  $\text{K}^+$  desorption processes, which again can be explained by the presence of different binding sites on the filament surface.

Concerning the use of the FR-SID approach to distinguish between Na and K in mixtures of different alkali salts, the filament temperature range 1400–1500 K seems to be optimal. In this range sodium desorption is fast enough to be detected and the rate constants of the two species deviate by approximately a factor of ten, which is large enough to make the contributions from Na and K separable.

The data for mixed NaCl/KCl particles was further analyzed to extract information about the relative content of the alkali metals in the particles. Integrals for the time range 0–1 s

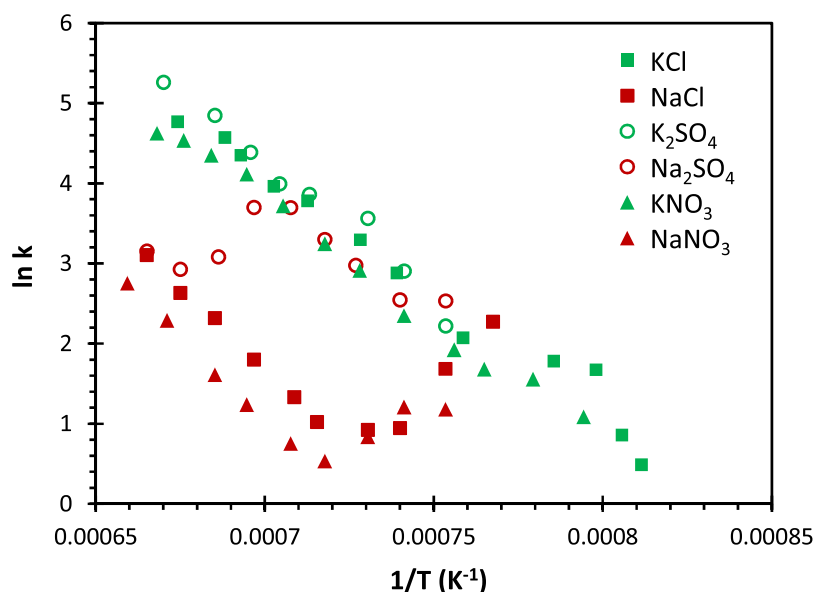


**Figure 9.** Arrhenius plot of desorption rate constants obtained in experiments with KCl, K<sub>2</sub>SO<sub>4</sub>, KNO<sub>3</sub>, NaCl, Na<sub>2</sub>SO<sub>4</sub> and NaNO<sub>3</sub> aerosol particles.

**Table 2.** Calculated Arrhenius parameters for alkali desorption from a polycrystalline platinum surface in air presented with standard deviation. Alkali salt particles with a diameter of 200 nm were continuously lead through the FR-SID during the experiments.

Salt	$E_a$ (eV)	$A$ (s <sup>-1</sup> )
KCl	$2.55 \pm 0.26$	$10^{(10.8 \pm 1.0)}$
NaCl	$3.51 \pm 0.21$	$10^{(13.1 \pm 0.7)}$
K <sub>2</sub> SO <sub>4</sub>	$2.96 \pm 0.49$	$10^{(12.3 \pm 1.8)}$
Na <sub>2</sub> SO <sub>4</sub>	—	—
KNO <sub>3</sub>	$2.60 \pm 0.20$	$10^{(10.8 \pm 0.7)}$
NaNO <sub>3</sub>	$3.38 \pm 0.45$	$10^{(12.4 \pm 1.6)}$

were calculated for each component in equation (8) using the following equation:

$$\int_0^t I_0 \cdot \exp(-k \cdot t) dt = I_0 \left[ \frac{\exp(-k \cdot t)}{-k} \right]_0^t = \frac{I_0}{k} (1 - e^{-k \cdot t}), \quad (9)$$

where  $k$  and  $I_0$  correspond to the derived values for each component and  $t = 1$  s. Obtained values were corrected for the lower  $\beta$  for Na compared to K (see equation (2)). The ratio between the calculated integrals was close to 1 in the filament temperature range 1400–1500 K, which shows that similar concentrations of Na and K have been detected in that interval. Since the original composition of Na and K atoms was 50:50, the results indicate that FR-SID can be applied to determine the relative mass concentrations of the two alkali species. At filament temperatures <1350 K the ratio deviated strongly from 1, which is expected since sodium is no longer efficiently detected at low temperatures.

FR-SID measurements were also performed using alkali sulfate and alkali nitrate particles. The decay curves were well described by the exponential function given in equation (5) and the obtained rate constant are summarized in figure 9, together with the previously presented alkali chloride data. Calculated Arrhenius parameters for the different systems are listed in table 2. The obtained rate constants and intensities for KNO<sub>3</sub> and NaNO<sub>3</sub> correlate well with the data for KCl and NaCl. The obtained rate constants for K<sub>2</sub>SO<sub>4</sub> were found to correlate with the data obtained for KCl, while the rate constants for Na<sub>2</sub>SO<sub>4</sub> started to shift towards the K values at a high filament temperature. The signal intensities for the sulfates were also lower than for the other salts and disappeared at a filament temperature of 1330 K (to be compared with 1230 K for KCl). Thus, the corresponding Na<sub>2</sub>SO<sub>4</sub> ion signal may be difficult to detect with the proposed technique. The lower sensitivity to sulfates is believed to be associated with the high thermal stability of alkali sulphates. To circumvent uncertainties induced by variations in alkali speciation a thermal preconditioning step may be suitable, discussed in further detail below.

The presented results suggest that Na and K concentrations (g m<sup>-3</sup>) can be derived using a FR-SID powered by a simple electronic support system and operating under atmospheric pressure. Future work should include statistical analysis of measurement uncertainties. Comparative measurements with laser instruments may also be beneficial to further explore solid-gas phase transition where the techniques potentially overlap. Regarding uncertainties, the surface temperature of the filament has a strong influence on the ion current amplitude and thereby also the obtained desorption coefficients. In the proposed application it is kept constant to ensure consistency and repeatability. The influence of possible oxidation and contamination of the platinum surface has been discussed in the literature and may influence the desorption kinetics

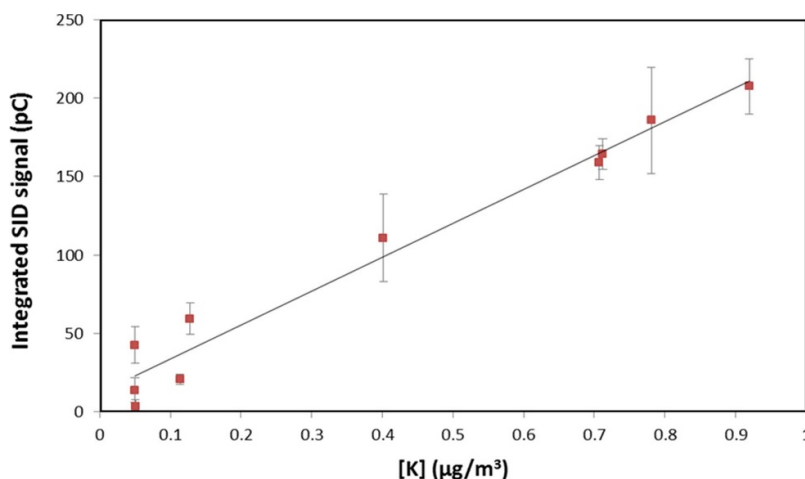


**Figure 10.** Measured integrated FR-SID signal as a function of mass concentration of K ( $\mu\text{g m}^{-3}$ ) based on KCl particles observed by conventional aerosol diagnostics. A linear least square calibration curve is fitted from the measurement points and the error bars represent the standard deviation of three consecutive measurements.

[29, 34, 35, 41]. However, throughout this work no apparent intensity reduction was observed between the initial and final measurements. The influence of particle diameter has also been studied and investigations with SI technique showed consistently decreased signals for larger particles, while the result for particle diameters  $<50$  nm is somewhat ambiguous [36, 42]. Thus, further assessment of particle size effects is needed.

In a first attempt to quantify the ion current the integrated desorption signal of  $\text{K}^+$  generated by KCl test aerosols, was compared with observed mass concentrations of conventional aerosol diagnostics (SMPS and optical spectrometry). At sufficient loadings ( $[\text{K}] > 0.2 \mu\text{g m}^{-3}$ ) a linear relation was observed with reasonable signal variance, shown in figure 10. At lower concentrations the signal-to-noise ratio becomes too low and disturbs the possibility to accurately report absolute concentrations for the simplified FR-SID unit described in this work. Note that the reference uncertainty, mainly refractive index, shape and density [43], are not considered. A similar calibration procedure has been used in previous research using continuously operated SI based diagnostics with acceptable deviations [24, 25, 44]. Recently, Gogolev *et al* found the SI instrument drift to be up to 1.5% per hour, omitting reference uncertainties [44]. To our knowledge, systematic uncertainties has not yet been reported in the literature and is a topic worthy of further investigations.

The results from the measurements with different alkali metal salts show that the FR-SID may be applied to distinguish between signals originating from Na and K, with the exception of  $\text{Na}_2\text{SO}_4$ , and thus serve as a valuable tool to address the accuracy of the similarity assumption for Na/K reactions with Cl and S-species. Other possible applications are investigations coupled to evaporation patterns from solid fuels and the Na/K vapor pressure in high temperature environments. Furthermore, techniques to distinguish between salts with different counter ions may also be worthy of further development. For example, a possible way to separate the more thermally stable sulfates from chlorides and nitrates could be by thermal

treatment of the inbound sample flow. Alkali chloride and nitrate particles would evaporate at a lower temperature and intact sulfate particles could hence be separated and passed on into the SID.

#### 4. Conclusions

Laboratory experiments have been performed to evaluate a new FR-SID instrument for real-time characterization of sodium and potassium containing aerosol particles. The combined FR and SI techniques is shown to allow differentiation between sodium and potassium based on their differences in desorption kinetics from a hot Pt surface.

Alkali desorption rate constants can be determined from ion signals that decay on the time scale of tens to hundreds of milliseconds, in contrast to earlier studies where the measured current has been observed to decay during a few milliseconds or faster [29]. The longer time scales simplify the experiments and the electronics required to operate the instrument. A filament temperature between 1400 K and 1500 K is concluded to be optimal for separation of signals due to Na and K. The observed differences in desorption kinetics for Na and K appears to be independent of counter ion for alkali chlorides and nitrates, whereas sulphate analysis was inhibited by the thermal stability of  $\text{Na}_2\text{SO}_4$ . Alkali chlorides and nitrates have similar detection efficiencies while the sensitivity to sulfates is lower, in agreement with earlier work [29]. Future methods to separate sulfates from other alkali salts may rely on differences in thermal stability of the compounds. Additional developments may also include the possibility to interchangeably carry out both particle mass and number concentration measurements with the same instrument.

This study hereby demonstrates proof-of-concept of the FR-SID technique and its applicability for discrete measurement of Na and K. A more thoroughly assessment of how particle morphology, size and chemical composition

influence the integrated desorption signal may be performed in connection to future field measurements.

## Acknowledgments

We gratefully acknowledge technical support from Benny Lönn and Torbjörn Gustavsson during the project. The Swedish Energy Agency is acknowledged for financial support.

## ORCID iD

Dan Gall  <https://orcid.org/0000-0003-3130-8377>

## References

- [1] ETSAP/IEA 2012 Biomass for heat and power: technology brief
- [2] Harb J N and Smith E E 1990 Fireside corrosion in pc-fired boilers *Prog. Energy Combust. Sci.* **16** 169–90
- [3] Pisa I and Lazaroiu G 2012 Influence of co-combustion of coal/biomass on the corrosion *Fuel Process. Technol.* **104** 356–64
- [4] Åmand L-E, Leckner B, Eskilsson D and Tullin C 2006 Ash deposition on heat transfer tubes during combustion of demolition wood *Energy Fuels* **20** 1001–7
- [5] Aho M, Envall T and Kauppinen J 2013 Corrosivity of flue gases during co-firing Chinese biomass with coal at fluidised bed conditions *Fuel Process. Technol.* **105** 82–8
- [6] Kassman H, Pettersson J, Steenari B-M and Åmand L-E 2013 Two strategies to reduce gaseous KCl and chlorine in deposits during biomass combustion— injection of ammonium sulphate and co-combustion with peat *Fuel Process. Technol.* **105** 170–80
- [7] Pettersson J, Svensson J-E and Johansson L-G 2008 Alkali induced corrosion of 304-type austenitic stainless steel at 600 °C; comparison between KCl, K<sub>2</sub>CO<sub>3</sub> and K<sub>2</sub>SO<sub>4</sub> vol 595–598 PA
- [8] Pettersson A, Elled A-L, Möller A, Steenari B-M and Åmand L-E 2009 The impact of zeolites during co-combustion of municipal sewage sludge with alkali and chlorine rich fuels *Proc. 20th Int. Conf. Fluid. Bed Combust* pp 902–9
- [9] Johansen J M, Jakobsen J G, Frandsen F J and Glarborg P 2011 Release of K, Cl, and S during pyrolysis and combustion of high-chlorine biomass *Energy Fuels* **25** 4961–71
- [10] Glarborg P 2007 Hidden interactions-trace species governing combustion and emissions *Proc. Combust. Inst.* **31** 1:77–98
- [11] Johansson L S, Tullin C, Leckner B and Sjövall P 2003 Particle emissions from biomass combustion in small combustors *Biomass Bioenergy* **25** 435–46
- [12] Knudsen J N, Jensen P A and Dam-Johansen K 2004 Transformation and release to the gas phase of Cl, K, and S during combustion of annual biomass *Energy Fuels* **18** 1385–99
- [13] Glarborg P and Marshall P 2005 Mechanism and modeling of the formation of gaseous alkali sulfates *Combust. Flame* **141** 22–39
- [14] Monkhouse P 2002 On-line diagnostic methods for metal species in industrial process gas *Prog. Energy Combust. Sci.* **28** 331–81
- [15] Forsberg C *et al* 2009 Principle, calibration and application of the *in-situ* alkali chloride monitor (IACM) *Rev. Sci. Instrum.* **80** 23104
- [16] Thorin E and Schmidt F M 2020 TDLAS-based photofragmentation spectroscopy for detection of K and KOH in flames under optically thick conditions *Opt. Lett.* **45** 5230–3
- [17] French R J and Milne T A 1994 Vapor phase release of alkali species in the combustion of biomass pyrolysis oils *Biomass Bioenergy* **7** 315–25
- [18] Viljanen J *et al* 2020 *In-situ* monitoring of transient gas phase K–Cl–S chemistry in a pilot-scale combustor *Proc. Combust. Inst.* **1–9**
- [19] Weng W, Brackmann C, Leffler T, Aldén M and Li Z 2019 Ultraviolet absorption cross sections of KOH and KCl for nonintrusive species-specific quantitative detection in hot flue gases *Anal. Chem.* **91** 4719–26
- [20] Viljanen J 2019 Online laser diagnostics for high-temperature chemistry in biomass combustion Doctoral Thesis (Tampere, Finland: Tampere University)
- [21] Ferge T *et al* 2005 On-line analysis of gas-phase composition in the combustion chamber and particle emission characteristics during combustion of wood and waste in a small batch reactor *Environ. Sci. Technol.* **39** 1393–402
- [22] Canagaratna M R *et al* 2007 Chemical and microphysical characterization of ambient aerosols with the aerodyne aerosol mass spectrometer *Mass Spectrom. Rev.* **26** 185–222
- [23] Sommersacher P, Kienzl N, Brunner T and Obernberger I 2016 Simultaneous online determination of S, Cl, K, Na Zn and Pb release from a single particle during biomass combustion part 2: results from test runs with spruce and straw pellets *Energy Fuels* **30** 3428–40
- [24] Gall D, Pushp M, Larsson A, Davidsson K and Pettersson J B C 2018 Online measurements of alkali metals during start-up and operation of an industrial-scale biomass gasification plant *Energy Fuels* **32** 532–41
- [25] Davidsson K O, Engvall K, Hagström M, Korsgren J G, Lönn B and Pettersson J B C 2002 A surface ionization instrument for on-line measurements of alkali metal components in combustion: instrument description and applications *Energy Fuels* **16** 1369–77
- [26] Gogolev I *et al* 2019 Chemical-looping combustion in a 100 kW unit using a mixture of synthetic and natural oxygen carriers—operational results and fate of biomass fuel alkali *Int. J. Greenh. Gas Control.* **88** 371–82
- [27] Pushp M, Gall D, Davidsson K, Seemann M and Pettersson J B C 2018 Influence of bed material, additives, and operational conditions on alkali metal and tar concentrations in fluidized bed gasification of biomass *Energy Fuels* **32** 6797–806
- [28] Wellinger M, Biollaz S, Wochele J and Ludwig C 2011 Sampling and online analysis of alkalis in thermal process gases with a novel surface ionization detector *Energy Fuels* **25** 4163–71
- [29] Hagström M, Jäglid U and Pettersson J B C 2000 Desorption kinetics at atmospheric pressure: alkali interactions with rhodium and steel surfaces *Appl. Surf. Sci.* **161** 291–9
- [30] Holmlid L and Olsson J 1977 Molecular beam surface ionization detection: II. Field reversal and surface ionization study of Na on Re with adsorbed oxygen *Surf. Sci.* **67** 61–76
- [31] Holmlid L and Olsson J O 1976 Simple surface ionization detector with field reversal for absolute ionization coefficient and ionic and neutral desorption measurements *Rev. Sci. Instrum.* **47** 1167–71
- [32] Kingdon K H 1923 A method for the neutralization of electron space charge by positive ionization at very low gas pressures *Phys. Rev.* **21** 408–18
- [33] Zandberg É Y and Ionov N 1959 Surface ionization *Usp. Fiz. Nauk* **57** 581–623
- [34] Möller K and Holmlid L 1985 Desorption of cesium from pyrolytic graphite basal surfaces with strongly non-equilibrium behaviour *Surf. Sci.* **163** L635–40

- [35] Stienkemeier F, Wewer M, Meier F and Lutz H O 2000 Langmuir–Taylor surface ionization of alkali (Li, Na, K) and alkaline earth (Ca, Sr, Ba) atoms attached to helium droplets *Rev. Sci. Instrum.* **71** 3480–4
- [36] Jäglid U, Olsson J G and Pettersson J B C 1996 Detection of sodium and potassium salt particles using surface ionization at atmospheric pressure *J. Aerosol. Sci.* **27** 967–77
- [37] Hagström M, Engvall K and Pettersson J B C 2000 Desorption kinetics at atmospheric pressure: alkali metal ion emission from hot platinum surfaces *J. Phys. Chem. B* **104** 4457–62
- [38] Möller K and Holmlid L 1988 Rate constants for cesium bulk diffusion and neutral desorption on pyrolytic graphite basal surfaces: a field reversal kinetic study *Surf. Sci.* **204** 98–112
- [39] Gall D, Pushp M, Davidsson K O and Pettersson J B C 2017 Online measurements of alkali and heavy tar components in biomass gasification *Energy Fuels* **31** 8152–61
- [40] Nordholm S 1985 Transition state analysis of preexponential factors in thermal desorption *Chem. Phys.* **98** 367–79
- [41] Kaminsky M 1965 Atomic and ionic impact phenomena on metal surfaces (<http://doi.org/10.1007/978-3-642-46025-8>)
- [42] Kowalski T, Ludwig C and Wokaun A 2007 Qualitative evaluation of alkali release during the pyrolysis of biomass *Energy Fuels* **21** 3017–22
- [43] McMurry P H 2000 A review of atmospheric aerosol measurements *Atmos. Environ.* **34** 1959–99
- [44] Gogolev I, Soleimanisalim A H, Linderholm C and Lyngfelt A 2021 Commissioning, performance benchmarking, and investigation of alkali emissions in a 10 kWth solid fuel chemical looping combustion pilot *Fuel* **287** 119530